# Modelling of micro-sources for security studies

Nikos D. Hatziargyriou, F. Kanellos, Georges Kariniotakis, Xavier Le Pivert, N. Jenkins, N. Jayawarna, Joao A. Pecas Lopes, J. Gil, C. Moreira, José Oyarzabal, et al.

HAL Id: hal-00529155

https://minesparis-psl.hal.science/hal-00529155

Submitted on 6 Feb 2018

# Modelling of Micro-Sources for Security Studies

N. HATZIARGYRIOU[*]     G. KARINIOTAKIS     N. JENKINS     J. PEÇAS LOPES     J. OYARZABAL
F. KANELLOS          X. LE  PIVERT       N. JAYAWARNA   N. GIL, C. MOREIRA   Z. LARRABE


National Technical     Ecole des Mines     UMIST          INESC Porto        LABEIN
University of Athens     de Paris
    **GREECE**            **FRANCE**          **UK**         **PORTUGAL**         **SPAIN**

**Abstract:** The interconnection of small, modular generation and storage technologies at the MV and LV distribution level have the potential to significantly impact power system performance. In this paper models of the main micro-generation sources are described. In particular, the models of Microturbines, Fuel Cells, Photovoltaic Systems and Wind Turbines, are described. In addition basic models of their power electronic interfaces are given. The integration of the above models in a steady state and dynamic simulation tool, which is developed in the framework of the EU funded MICROGRIDS project, will provide a simulation test platform, which will be necessary to define and evaluate the developed operational and control strategies.

**Keywords**: Microgrids, Wind Turbines, Fuel Cells, Photovoltaic Systems, Micro-turbines, Control Systems.

## 1. INTRODUCTION

Small, modular generation technologies interconnected to low-voltage (LV) distribution systems have the potential to form a new type of power system, the MicroGrid [1, 2]. MicroGrids can be connected to the main power network or be operated autonomously, if they are operated from the power grid, in a similar manner to the power systems of physical islands. The microgenerators are small units of less than 100 kWs, most of them with power electronic interface, using either Renewable Energy Sources or fossil fuel in high efficiency local co-generation mode. Both of these technologies are critical to reducing Europe's GHG emissions and dependence on imported fossil fuel, where the MicroGrid concept will allow their most effective implementation.

MicroGrids may use single-phase circuits and be loaded with single-phase loads. These factors generate unbalanced conditions that can be accentuated with the interaction of dynamic loads such as induction motors. To model these effects, analysis tools must model the system with its three phases, the neutral conductors, the ground conductors and the connections to ground. The developed analytical tool should include steady state and dynamic models for the various forms of micro-sources and their interfaces.

In the EU funded MICROGRIDS project [1] a simulation platform able to simulate the steady state and dynamic operation of LV three-phase networks that include micro generation sources is under development. This involves the development of adequate models in the time range of ms of the micro sources, machines (induction and synchronous machines) and inverters [3]. Normally these devices are directly coupled to the grid and thus have a direct impact on the grid voltage and frequency. In this paper the following models are described:

- Induction Generators
- Micro-turbines
- Photovoltaic Systems

---

[*] nh@power.ece.ntua.gr

- Fuel Cells
- Wind Turbines
- Grid-side inverter generic model.

## 2. INDUCTION GENERATORS

**Three-Phase Symmetrical Induction Generator**

Induction machines are represented by the fourth order model expressed in the arbitrary reference frame. Using generator convention for the stator currents [3, 4]:

$$u_{sd} = -r_s \cdot i_{sd} - \omega \cdot \Psi_{sq} + p\Psi_{sd}$$

$$u_{sq} = -r_s \cdot i_{sq} + \omega \cdot \Psi_{sd} + p\Psi_{sq} \tag{1}$$

$$u_{rd} = r_r \cdot i_{rd} - (\omega - \omega_r) \cdot \Psi_{rq} + p\Psi_{rd}$$

$$u_{rq} = r_r \cdot i_{rq} + (\omega - \omega_r) \cdot \Psi_{rd} + p\Psi_{rq}$$

$p = \dfrac{1}{\omega_o}\dfrac{d}{dt}$, $\omega_o$ is the base cyclic frequency, $\omega$ is the rotating speed of the arbitrary reference frame and subscripts *{d}, {q}, {s}, {r}* denote *dq*-axis, stator, rotor, respectively.

The fluxes are related to the stator, rotor winding currents by the following equations,

$$\Psi_{sd} = -X_s \cdot i_{sd} + X_m \cdot i_{rd}$$

$$\Psi_{sq} = -X_s \cdot i_{sq} + X_m \cdot i_{rq}$$

$$\Psi_{rd} = -X_m \cdot i_{sd} + X_r \cdot i_{rd} \tag{2}$$

$$\Psi_{rq} = -X_m \cdot i_{sq} + X_r \cdot i_{rq}$$

The electromagnetic torque is given by:

$$T_e = \Psi_{qr} \cdot i_{dr} - \Psi_{dr} \cdot i_{qr} \tag{3}$$

**Single-Phase Induction Generator**

The dynamic model of a single-phase induction machine in the stator reference frame is described next. All quantities are referred to the *main* winding (denoted by the use of double prime).

$$v_{qs} = R_{1m} \cdot i_{qs} + p\Psi_{qs}$$

$$v'_{qr} = R_{2m} \cdot i'_{qr} - \omega_r \cdot \Psi''_{dr} + p\Psi'_{qr} \tag{4}$$

$$v''_{dr} = R_{2m} \cdot i''_{dr} + \omega_r \cdot \Psi'_{qr} + p\Psi''_{dr}$$

$$\Psi_{qs} = X_{1m} \cdot i_{qs} + X_{Mm}(i_{qs} + i'_{qr})$$

$$\Psi'_{qr} = X_{2m} \cdot i'_{qr} + X_{Mm}(i_{qs} + i'_{qr})$$

$$\Psi''_{dr} = (X_{2m} + X_{Mm})i''_{dr} \tag{5}$$

$$i''_{dr} = \frac{N_a}{N_m} i'_{dr}$$

Subscript *{m}* denotes *m* winding. The electromagnetic torque is given by:

$$T_e = \frac{P}{2}(\lambda'_{qr} \cdot i''_{dr} - \lambda''_{dr} \cdot i'_{qr}) \tag{6}$$

## 3. MICROTURBINES

Microturbines are small and simple-cycle gas turbines with outputs ranging typically from around 25 to 300 *kW*. They are part of a general evolution in gas turbine technology. Techniques incorporated into the larger machines, to improve performance, can be typically found in microturbines as well. These include recuperation, low $NO_X$ emission technologies, and the use of advanced materials, such as ceramics, for the hot section parts [5].

There are essentially two types of microturbines. One is a high-speed single-shaft unit with a compressor and turbine mounted on the same shaft as an electrical synchronous machine. In this case turbine speeds mainly range from 50.000 to 120.000 *rpm*. The other type of microturbines is a split-shaft designed one that uses a power turbine rotating at 3000 rpm and a conventional generator connected via a gearbox. In typical microturbine designs, this micro-generation system is composed of the following main parts:

*Turbine and Recuperator*: The primary machine is a small gas turbine. The recuperator is a heat exchanger, which transfers heat from the exhaust gas to the discharge air before it enters the combustor. This reduces the amount of fuel required to raise the discharge air temperature to that required by the turbine.

*Electrical generator*: In the single-shaft design, a synchronous generator is directly coupled to the single shaft turbine. The rotor is either a two- or four-pole permanent magnet with a stator that presents a conventional copper wound design. In the split-shaft design, a conventional induction or synchronous machine is mounted on the power turbine via a gearbox.

*Power electronics*: In the single-shaft design, the alternator generates a very high frequency three- phase voltage ranging from 1500 to 4000 *Hz*. To allow grid interconnection, the high frequency voltage needs to be first rectified and then inverted to a normal 50 *Hz* voltage. In the split-shaft turbine design, power inverters are not needed since the generator is directly coupled to the grid.

Since in this research we are mainly interested in the dynamic performance of the network and not the fast transients that may happen, the microturbine model adopted is based on the following assumptions:

1) The recuperator is not included in the model since it is mainly used to raise engine efficiency.

2) The gas turbine's temperature control and the acceleration control have no impact in normal operating conditions. Therefore they can be omitted in the turbine model.

A simplified block diagram for the microturbine for load following dynamic behaviour analysis purposes is shown in figure 1. The details of these control blocks with all parameters are given next.
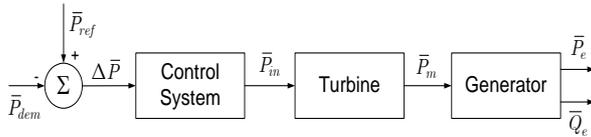


**Figure 1.** *Main blocks in microturbine model*
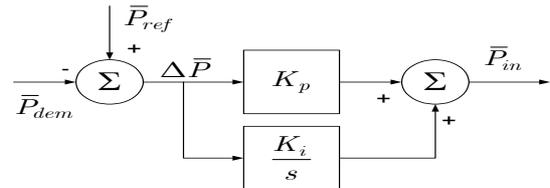


**Figure 2**. Load following control system model.

The real power control can be described as a proportional-integral (PI) control function as shown in figure 2. The real power control variable $P_{in}$ is then applied to the turbine. $P_{dem}$ is the demanded power, $P_{ref}$ is the reference power, $P_{in}$ is the power control variable to be applied to the turbine, $K_p$ is the proportional gain and $K_i$ is the integral gain in the PI controller.

**Turbine**

The *GAST* turbine model is one of the most commonly used dynamic models of gas turbine units [6]. The model is simple and follows typical modelling guidelines [7]. Therefore the turbine part in this microturbine design is modelled as *GAST* model.
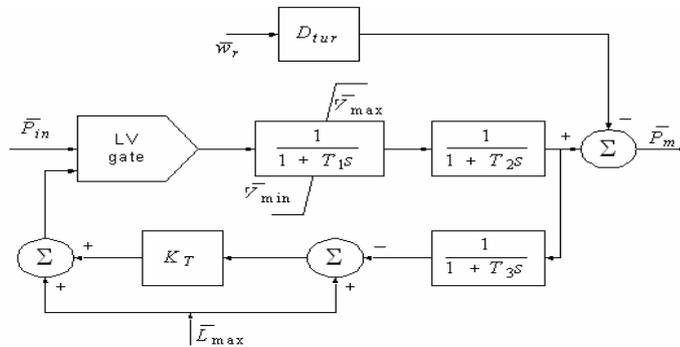


**Figure 3.** Turbine model.

$P_m$ is the mechanical power, $D_{tur}$ is the damping of turbine, $T_1$ is the fuel system lag time constant 1, $T_2$ is the fuel system lag time constant 2, $T_3$ is the load limit time constant, $L_{max}$ is the load limit, $V_{max}$ is the maximum value position, $V_{min}$ is the minimum value position, $K_T$ is the temperature control loop gain.

In the microturbines that are designed to operate in stand alone conditions a battery is connected to the dc link to help providing fast response to load increases. The interface with the grid is also provided by an inverter.

## 4. PHOTOVOLTAIC SYSTEMS

### PV Array models

Many models of varying complexity describing the behaviour of a PV cell/module/array exist. To choose an appropriate model for simulation, several factors need to be considered. The most important one is accuracy. There is always a trade-off between accuracy and simplicity. To minimise the computational effort which is involved in simulating microgrids the model should be kept as simple as possible without sacrificing the required accuracy.

In contrast to the utility grid, a PV cell/module/array is not a fixed voltage source. Simulation requires the model to be able to predict current and voltage over the entire operating voltage range. Another factor is whether the data needed to drive the model is available, i.e. if data can be obtained in the relevant literature and/or manufacturers publications.

Two analytical models [8, 9] are proposed in this paper. The Simplified Single-Diode Model is a PV model that only characterises the behaviour of the PV Modules of a PV Plant. If a PV Plant is going to be modelled, a MPPT and an inverter model will be necessary. The PV Array with integrated MPPT model, is a very simple model based on the hypothesis that the PV modules are always working in its maximum power point.

### Simplified Single-Diode Model

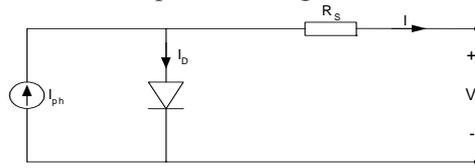A solar cell is represented by an electrical equivalent single-diode model [8] as the one shown in figure 4.



**Figure 4.** Simplified single-diode model of a solar cell.

The model inputs are the ambient temperature, solar irradiance, array voltage while the output of the model is array current. Voltage will be an input from the MPPT control scheme embedded in the inverter.

It is assumed that:

- All the cells of the module are identical and they work with the same irradiance and temperature. Also, voltage drops in the conductors that interconnect the cells are negligible.
- Short circuit current is affected only by the irradiance and temperature of the solar cells.
- Open circuit voltage of the cells depends exclusively on the temperature of the solar cells.
- Temperature of the solar cells depends exclusively on the irradiance and ambient temperature.
- Series resistance and diode quality factor of the cells are considered constant for all operating temperature and irradiance range.

The PV module's current $I^M$ under arbitrary operating conditions can be described as:

$$I^M = I_{SC}^M \cdot \left[ 1 - e^{\frac{V^M - V_{OC}^M + I^M \cdot R_S^M}{V_t^M}} \right] \tag{7}$$

where,

$$
\left.
\begin{aligned}
I_{SC}^M &= \frac{G_a}{G_{a0}} \cdot \left[ I_{SC,0}^M + \mu_{I_{SC}} \cdot (T_C - T_{C,0}) \right] \\
V_{OC}^M &= V_{OC,0}^M + \mu_{V_{OC}} \cdot (T_C - T_{C,0}) \\
V_t^M &= N_{SM} \cdot m \cdot \frac{k \cdot T_C}{e}
\end{aligned}
\right\}
\text{where } T_C = T_a + G_a \cdot \frac{NOCT - 20}{800}
$$

$$
R_S^M = R_S^C \cdot \frac{N_{SM}}{N_{PM}} \quad \text{where } R_S^C = \left| r_s \right| \cdot \frac{V_{OC,0}^C}{I_{SC,0}^C} \Rightarrow
$$

$$
\Rightarrow
\left\{
\begin{aligned}
&V_{OC,0}^C = \frac{V_{OC,0}^M}{N_{SM}}, \quad I_{SC,0}^C = \frac{I_{SC,0}^M}{N_{PM}} \\
&\left\{
\begin{aligned}
FF &= \frac{v_{OC,0} - \ln(v_{OC,0} + 0.72)}{v_{OC,0} + 1} \Rightarrow v_{OC,0} = \frac{V_{OC,0}^C}{V_{t,0}^C} \Rightarrow V_{t,0}^C = m \cdot \frac{k \cdot T_{C,0}}{e} \\
r_s &= 1 - \frac{FF}{FF_0} \Rightarrow \\
FF_0 &= \frac{P_{max,0}^C}{V_{OC,0}^C \cdot I_{SC,0}^C} \Rightarrow P_{max,0}^C = \frac{P_{max,0}^M}{N_{SM} \cdot N_{PM}}
\end{aligned}
\right.
\end{aligned}
\right.
$$

Once the module's current and voltage for operating conditions have been determined, the current and voltage of the PV Array are calculated:

$$I^A = N_{PA} \cdot I^M$$
$$V^A = N_{SA} \cdot V^M \tag{8}$$

The model parameters are given next:

$I^M$: Module current

$V^M$: Module voltage.

$R_{SM}$: Module series resistance.

$I_{SC}^M$: Short circuit current of the module.

$V_{OC}^M$: Open circuit voltage of the module.

$V_t^M$: Thermal voltage in the module.

$I_{max,0}^M$: Module current at standard conditions.

$V_{max,0}^M$: Module voltage at standard conditions.

$P_{max,0}^M$: Module maximum power at standard conditions.

$I_{SC,0}^M$: Module short circuit current at standard conditions.

$V_{OC,0}^M$: Module open-circuit voltage at standard conditions.

$N_{SM}$: Module number of cells in series.

$N_{PM}$: Module number of cells in parallel.

$NOCT$: Module normal operating cell temperature.

$\mu_{I_{SC}}$: Module short circuit current variation coefficient with temperature.

$\mu_{V_{OC}}$: Module open circuit voltage variation coefficient with temperature.

$m$: Module diode quality factor.

**PV Array with integrated MPPT model**

This is a very simple model that considers that the PV Array is working always at its maximum power point for given temperature and irradiance conditions. The model inputs are ambient temperature and solar irradiance while its output is array maximum power.

It is assumed that:

▪ All the cells of the PV Array are identical and they work with the same irradiance and temperature.
▪ No losses in the PV Array with MPPT system
▪ The PV Array is always working on its maximum power point for given irradiance and ambient temperature conditions.
▪ If irradiance and ambient temperature conditions change, the model instantaneously changes its maximum power point.
▪ Temperature of the solar cells depends exclusively on the irradiance and ambient temperature.

This model is based on the linear variation of a PV module power with its temperature. Substituting the module temperature by irradiance and ambient temperature, and multiplying the power with the number of modules of the array, we obtain:

$$\left. \begin{array}{l} P_{Max}^M = P_{Max0}^M + \mu_{P_{Max}} \cdot \left(T_M - T_{M,0}\right) \\ T_M = T_a + G_a \cdot \dfrac{NOCT-20}{800} \end{array} \right\} \Rightarrow$$

$$\Rightarrow P_{Max} = N \cdot \left[ P_{Max0}^M + \mu_{P_{Max}} \cdot \left(T_a + G_a \cdot \dfrac{NOCT-20}{800} - 25\right) \right] \tag{9}$$

Where,

$\mu_{P_{Max}}$: Module power variation coefficient with temperature.

$N$: Number of modules of the PV Array.

$P_{Max}^M$: PV Module Maximum Power.

$T_M$: Module Temperature.

$T_{M,0}$: Module Temperature at standard conditions.

$T_a$: Ambient Temperature.

$G_a$: Irradiance.

### 5. FUEL CELLS

Nowadays there are available five different types of Fuel Cells:
- *AFC* – Alcaline Fuel Cell;
- *PEFC/PEM* – Polymer Electrolyte Fuel Cell / Proton Exchange Membrane;
- *PAFC* – Phosphoric Acid Fuel Cell;
- *MCFC* – Molten Carbonate Fuel Cell;
- *SOFC* – Solid Oxid Fuel Cell.

The Solid Oxide Fuel Cell (*SOFC*) technology offers higher efficiencies and provides a great amount of heat (with high operating temperature - between 600 and 1000 ℃) turning into an interesting technology for cogeneration and more specifically residential-building scale distributed generation. The *SOFC* model is described in this paper. A power generation fuel cell system has the following three main parts:

*Fuel processor* The fuel processor converts fuels such as natural gas to hydrogen and by product gases.

*Power section* The power section generates the electricity. There are numerous individual electrochemical fuel cells in the power section.

*Power conditioner* The power conditioner converts *dc* power to ac power output and includes current, voltage and frequency control.

**Fuel Cell Modelling**

It is assumed that the anode is supplied with $H_2$ only and the cathode with $O_2$ only, so that the only reaction that occurs in the fuel cell is:

$$H_2 + \frac{1}{2}O_2 \rightarrow H_2O \tag{10}$$

The potential difference between the anode and the cathode is calculated using the *Nernst's* equation and *Ohm's* law:

$$V_{fc}^r = N_0 \cdot [E_0 + \frac{R \cdot T}{2F}(\ln \frac{p_{H_2O} \cdot p_{O_2}^{1/2}}{p_{H_2O}})] - r \cdot I_{fc}^r \tag{11}$$

Where, $E_0$ is the voltage associated with reaction free energy (V), $p_{H_2}$, $p_{O_2}$, $p_{H_2O}$ are the partial pressures of the component ($N/m^2$), $N_0$ is the number of cells, $r$ is the electrical resistance of the fuel cell ($\Omega$), $I_{fc}^r$ is the reaction current or the output current (*A*), *R* is the universal gas constant (*J/mol K*), *T* is the channel temperature (*K*), *F* is the Faraday's constant (*Coulombs/mol*).

The partial pressure of the components is related to its molar flow. The ideal gas law leads to the following relationship:

$$p_i \cdot V_{ch} = n_i \cdot R \cdot T \tag{12}$$

Where, $V_{ch}$ is the volume of the channel ($m^3$) and $n_i$ is the number of moles of the element *i* (*moles*).

The following differential equations describe the chemical behaviour of the reactions:

$$\frac{dp_i}{dt} = \frac{R \cdot T}{V_{ch}} \frac{dn_i}{dt} \tag{13}$$

and

$$\frac{dn_i}{dt} = q_i^{ch} = (q_i^{in} - q_i^r) \tag{14}$$

Where, $q_i^{in}$ is the flow of the $i_{th}$ element of input, $q_i^r$ is the flow of $i_{th}$ element that reacts.

For the $H_2$ the value of $q_i^r$ we have:

$$q_{H_2}^r = \frac{N_0 \cdot I_{fc}^r}{2F} = 2K_r I_{fc}^r \tag{15}$$

The values of $q^r$ for the other elements are such that:

$$q_{O_2}^r = \frac{q_{H_2}^r}{2} = K_r I_{fc}^r \tag{16}$$

$$q^r_{H_2O} = q^r_{H_2} = 2K_rI^r_{fc} \qquad (17)$$

Defining the fuel utilisation $U_f$, as the ratio between the fuel flow that reacts and the input fuel flow and assuming a typical use between 80 and 90% as described in [7], the demand current of the fuel cell system can be restricted in the range given by:

$$\frac{0.8q^{in}_{H_2}}{2K_r} \le I^r_{fc} \le \frac{0.9q^{in}_{H_2}}{2K_r} \qquad (18)$$

The optimal utilisation factor ($U_{opt}$) is assumed to be 85%, allowing the control of the input fuel flow by measuring the output current, so that:

$$q^{in}_{H_2} = \frac{2K_rI^r_{fc}}{0.85} \qquad (19)$$

The stichiometric ratio of hydrogen to oxygen is 2 to 1. Oxygen excess is always taken in, to let hydrogen react with oxygen more completely. According to [7], under normal operation the value of $r_{H_2O}$ should be 1.145, in order to keep the fuel cell pressure difference below 4 $kPa$. So the input oxygen flow, $q^{in}_{O_2}$, is controlled to keep $r_{H_2O}$ at 1.145 by controlling the speed of the air compressor.

$$q^{in}_{O_2} = r_{H_2O} \cdot q^{in}_{H_2} \qquad (20)$$

All the reactions that occur in the fuel cell have some time delay associated. The chemical response in the fuel processor is usually slow, as it is associated with the time to change the chemical reaction parameters after a change in the flow of reactants. This dynamic response function is modelled as a first-order transfer function with a 5s time delay constant ($T_f$). The electrical response time delay in the fuel cells is generally short and mainly associated with the speed at which the chemical reaction is capable of restoring the charge that has been drained by the load. This dynamic response function is also modelled as a first-order transfer function, but with a 0.8s time delay constant ($T_e$). The dynamic response function of the flow is also modelled as a first-order transfer function with the time delay constant of the respective element, $\tau_{H_2}$, for the response time of hydrogen flow, $\tau_{O2}$ for oxygen and $\tau_{H_2O}$ for water flow, as described in [7]. The outputs of this model provide the potential difference between anode and cathode and $I^r_{fc}$ the reaction current. A conventional battery can be connected to the *dc* output of the fuel cell to provide fast response to load step increases.

The interface with the grid is made through an inverter that may include a power frequency control loop for stand alone operation.

## 6. WIND TURBINES

Wind Turbines comprise several subsystems that are modelled independently. These subsystems are the aerodynamic, the generator, the mechanical and the power converters in case of variable speed wind turbines. The models of each subsystem are described next.

**Aerodynamic subsystem**

The aerodynamic coefficient curves are used for the study of the blades dynamics [1, 3]:

$$P_a = \omega_r \cdot T_w = \frac{1}{2} \cdot \rho \cdot A \cdot C_p(\lambda, \beta) \cdot v^3_w \qquad (21)$$

$P_a$ is the aerodynamic power, $C_p(\lambda,\beta)$ is the dimensionless performance coefficient, $\lambda$ is the tip speed ratio, $\beta$ is the pitch angle, $\rho$ is the air density, $A=\pi R^2$ is the rotor area, $v_w$ is the wind speed, $\omega_r$ is the blade rotating speed and $T_w$ the aerodynamic torque.

In order to reproduce the rotor aerodynamic torque harmonics due to the tower shadow and wind shear effects, each blade must be modeled independently. The tower shadow is approximated by considering a near sinusoidal reduction of the equivalent blade wind speed, as each blade passes in front of the tower.

**Mechanical subsystem**

The equivalents of three or six elastically connected masses can be optionally used for simulating the mechanical system of the WT. The use of at least two masses is necessary for the representation of the low-

speed shaft torsional mode. In case of the three-mass equivalent, the state space equations of the model are the following [3, 4]:

$$\frac{d}{dt}\begin{bmatrix}\theta\\\omega\end{bmatrix}=\begin{bmatrix}[0]_{3\times3} & [I]_{3\times3}\\-\frac{1}{2}[H]^{-1}[C] & -\frac{1}{2}[H]^{-1}[D]\end{bmatrix}\begin{bmatrix}\theta\\\omega\end{bmatrix}+\begin{bmatrix}[0]_{3\times3}\\\frac{1}{2}[H]^{-1}\end{bmatrix}T \tag{22}$$

Where $\theta^T=[\theta_R,\theta_{GB},\theta_G]$ is the angular position vector, $\omega^T=[\omega_R,\omega_{GB},\omega_G]$ is the angular speed vector and $T^T=[T_W,0,T_G]$ is the external torque vector comprising the aerodynamic and the electromagnetic torque, $T_w$ and $T_G$. $[0]_{3x3}$, $[I]_{3x3}$ are the zero and identity *3x3* matrices, respectively. $[H]=diag(H_R,H_{GB},H_G)$ is the diagonal inertia matrix, $C$ is the stiffness matrix and $D$ is the damping matrix. $C$ matrix represents the low and high-speed shaft elasticities and is defined by $[C]=\begin{bmatrix}C_{HGB} & -C_{HBG} & 0\\-C_{HBG} & C_{HBG}+C_{GBG} & -C_{GBG}\\0 & -C_{GBG} & C_{GBG}\end{bmatrix}$, while

$[D]=\begin{bmatrix}D_R+d_{HGB} & -d_{HGB} & 0\\-d_{HGB} & D_{GB}+d_{HGB}+d_{GBG} & -d_{GBG}\\0 & -d_{GBG} & D_G+d_{GBG}\end{bmatrix}$ and represents the internal friction and the torque losses. Subscripts

*{gb}, {g}* denote gear-box and generator, respectively.

**Induction Generator Controller**

In figure 5 the simplified block-diagram of a typical scalar control system is shown. $V_s$ and $\omega_e$ are the stator voltage and frequency that is the magnitude and frequency of the inverter ac voltage. The frequency control subsystem basically consists of the PI speed controller. The rotor speed reference, $\omega_r*$, is externally determined by the optimal control characteristic of the turbine rotor. Output of the speed controller is the slip frequency, $\omega_{sl}$, which is added to the rotor speed, to determine the stator frequency $\omega_e$. For regulating the generator voltage, the constant *V/f* control principle is employed. It must be noted that practical control systems of this type may comprise several additional blocks (stabilizers, limiters *etc*.), which have to be included in the dynamic model of the system.
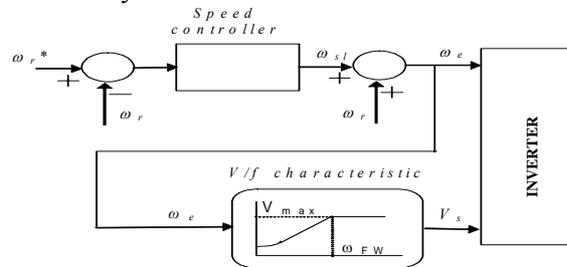


**Figure 5.** Scalar control system of the generator-side converter.

**6. GRID-SIDE INVERTER**

The circuit diagram of a *VSC* is shown in figure 6 and the symbols used are as follows:

$[e]=\begin{bmatrix}e_a & e_b & e_c\end{bmatrix}^T$ are the *ac* source phase voltages, $[i]=\begin{bmatrix}i_a & i_b & i_c\end{bmatrix}^T$ are the source currents, $[v]=\begin{bmatrix}v_a & v_b & v_c\end{bmatrix}^T$ are the ac side terminal voltages (fundamental component). *R, L* are the resistance and inductance of ac side series *R-L* circuit, $C_{dc}$ is the smoothing capacitance and $v_{dc},i_{dc}$ are the *dc* side voltage and current, respectively.
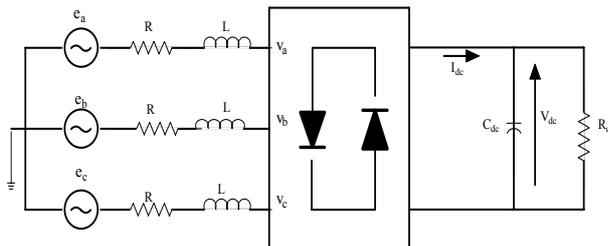


**Figure 6.** Circuit diagram of three-phase *VSC*

The generic model of a *VSC* [10] is described next. All model variables are transformed in to the synchronous orthogonal reference frame rotating at the supply frequency using *Clarke's* transformation. $[E] = \begin{bmatrix} E_d & E_q \end{bmatrix}^T, and [V] = \begin{bmatrix} V_d & V_q \end{bmatrix}^T$ are the voltages in *d-q* reference frame, $[I] = \begin{bmatrix} I_d & I_q \end{bmatrix}^T$ are the currents in *d-q* reference frame while $\omega$ is the angular frequency of the ac voltage source.

The active power absorbed from the *ac* source

$$P_{ac} = \frac{3}{2} \times E_d \times I_d + \frac{3}{2} \times E_q \times I_q \tag{23}$$

Active power delivered to the converter *dc* side is given by:

$$P_{dc} = V_{dc} \times I_{dc} = C_{dc} \times V_{dc} \times \frac{d}{dt} V_{dc} + \frac{1}{R_{dc}} \times V_{dc}^2 \tag{24}$$

$$P_{ac} = P_{dc} + P_{loss} \tag{25}$$

We can neglect the converter loss without loss of accuracy. Then

$$C_{dc} \times V_{dc} \frac{d}{dt} V_{dc} + \frac{1}{R_{dc}} \times V_{dc}^2 = \frac{3}{2} \times E_d \times V_d + \frac{3}{2} \times E_q \times I_q \tag{26}$$

Which could be arranged as,

$$\frac{d}{dt}\left(V_{dc}^2\right) = -\frac{2}{R_{dc} \times C_{dc}} \times \left(V_{dc}^2\right) + \frac{3 \times E_d}{C_{dc}} \times I_d + \frac{3 \times E_q}{C_{dc}} \times I_q \tag{27}$$

This could also be written as,

$$\frac{d}{dt}\left(V_{dc}^2\right) = k_d \times I_d + k_q \times I_q + k_c \times \left(V_{dc}^2\right) \tag{28}$$

where, $k_d = \dfrac{3 \times E_d}{C_{dc}}, k_q = \dfrac{3 \times E_q}{C_{dc}} and, k_c = -\dfrac{2}{R_{dc} \times C_{dc}}$

When $V_{dc}^2$ is taken as the state variable, instead of $V_{dc}$, this becomes a linear equation. Thus the state-space model including capacitor dynamics could be represented by the following sets of matrices.

$$\frac{d}{dt}\begin{bmatrix} I_d \\ I_q \\ (V_{dc}^2) \end{bmatrix} = \begin{bmatrix} -R/L & \omega & 0 \\ -\omega & -R/L & 0 \\ k_d & k_q & k_c \end{bmatrix} \begin{bmatrix} I_d \\ I_q \\ (V_{dc}^2) \end{bmatrix} + \begin{bmatrix} 1/L & 0 & 0 \\ 0 & 1/L & 0 \\ 0 & 0 & 0 \end{bmatrix} \begin{bmatrix} U_d \\ U_q \\ 0 \end{bmatrix} \tag{29}$$

$$y = \begin{bmatrix} 1 & 0 & 0 \\ 0 & 1 & 0 \\ 0 & 0 & 1 \end{bmatrix} \begin{bmatrix} I_d \\ I_q \\ (V_{dc}^2) \end{bmatrix} \tag{30}$$

$I_d, I_q, \left(V_{dc}^2\right)$ are the state variables and output variables while $U_d, U_q$ are the input variables of the model.

**Control system**

The control system model has two inputs, phase angle and reactive power. Both are fed in by the main system. A three-phase Phase Locked Loop gives out three outputs.
1. Measured frequency in Hz
2. Ramp, $\omega \times t$ which varied between 0 and 2*pi
3. The vector $\begin{bmatrix} \sin(\omega t) & \cos(\omega t) \end{bmatrix}$

The magnitude of *V* is obtained by regulation of reactive power; *Q*. Using *E* and *V*, values for $U_{abc}$ are obtained. $\left([U_{abc}] = [E_{abc}] - [V_{abc}]\right)$. $U_{abc}$ is transformed into $U_d$ and $U_q$ using *Park's* transformation to obtain the inputs for the state-space model.

**7. CONCLUSIONS**

In this paper models of various Microsources are described. These include models of Wind Turbines, Photovoltaic Systems, Fuel Cells and Microturbines and basic models of power electronic interfaces. The integration of the above models in a steady state and dynamic simulation tool will provide a simulation platform in order to test isolated and interconnected control and operation strategies of LV microgrids.

**8. BIBLIOGRAPHY**

[1] "MICROGRIDS – Large Scale Integration of Micro-Generation to Low Voltage Grids", EU Contract ENK5-CT-2002-00610, Technical Annex, May 2002,
    also http://microgrids.power.ece.ntua.gr
[2] "The CERTS Microgrid Concept", White paper on Integration of Distributed Energy Resources, R. Lasseter at al, April 2002
[3] Technical Brochure CIGRE Task Force 38.01.10, "Modelling New Forms of Generation and Storage", Nov. 2000.
[4] F. D. Kanellos, N.D. Hatziargyriou, "The Effect of Variable Speed Wind Turbines on the Operation of Weak Distribution Networks", *IEEE Trans. on Energy Conversion*, vol: 17, issue: 4, pages: 543 -548, December 2002.
[5] J.H. Watts, "Microturbines: a new class of gas turbine engines", *Gas Turbine News in Brief 39* (1), 5-11, 1999.
[6] M. Nagpal, A. Moshref, G.K. Morison, et al., "Experience with testing and modelling of gas turbines", *Proc. of the IEEE/PES 2001 Winter Meeting*, pp. 652-656, Jan./Feb. 2001,Columbus, Ohio, USA.
[7] Y. Zhu, K. Tomsovic, "Development if models for analysing load-following performance of microturbines and fuel cells", *Electric Power Systems Research 62*, 1-11, 2002.
[8] J. C. H. Phang, D. S. H. Chan, J. R. Phillips, "Accurate Analytical Method for the Extraction of Solar Cell Model Parameters", *Electronics Letters,* 10th May 1984 Vol. 20 No. 10, pp. 406-408.
[9] D. L. King, "Photovoltaic Module and Array Performance Characterization Methods for All System Operating Conditions," *NREL/SNL Program Review,* AIP Press, 1996, pp.347-368.
[10] Schauder, C., Mehta, H., "Vector Analysis and Control of Advanced Static VAR compensators", *IEE PROCEEDINGS-C,* Vol. 140, No.4, July 1993.